# Anomalous $WW\gamma$ vertex in $\gamma e$ collision with polarized beams

S. Atağ* and İ. Şahin
*Ankara University Department of Physics, Faculty of Sciences, 06100 Tandogan, Ankara, Turkey*
(Received 29 April 2001; revised manuscript received 29 June 2001; published 12 September 2001)

The potential of the $\gamma e$ mode of a linear $e^+e^-$ collider to probe the $WW\gamma$ vertex is investigated through the $W$ boson production angular distribution from the process $\gamma e \to W\nu$. Considering the longitudinal and transverse polarization states of the $W$ and incoming polarized beams we find the 95% C.L. limits of $-0.0003 < \Delta\kappa < 0.0003$, $-0.0006 < \lambda < 0.0006$, with an integrated luminosity of 500 $\text{fb}^{-1}$, $\sqrt{s}=1$ TeV and without any systematic uncertainty. It is shown that the polarization can improve the sensitivity to $\Delta\kappa$ by a factor of 1.3 and to $\lambda$ by factors of 2.8–10 depending on the energy.

DOI: 10.1103/PhysRevD.64.095002 PACS number(s): 12.60.−i, 13.88.+e, 14.70.−e

## I. INTRODUCTION

Recently there have been intensive studies to test the deviations from the standard model (SM) at present and future colliders. The investigation of three gauge boson couplings plays an important role to manifest the non-Abelian gauge symmetry in standard electroweak theory. The precision measurement of the triple vector boson vertices will be the crucial test of the structure of the SM.

Measurements at the Fermilab Tevatron and CERN $e^+e^-$ collider LEP2 provide present collider limits on anomalous couplings. Recent results from the D0 Collaboration for $WW\gamma$ couplings are given by $-0.25 < \Delta\kappa < 0.39$ ($\lambda=0$) and $-0.18 < \lambda < 0.19$ ($\Delta\kappa=0$) at 95% C.L., assuming the $WW\gamma$ couplings are equal to the $WWZ$ couplings [1]. Individual experiments by the ALEPH, DELPHI, L3, and OPAL Collaborations at LEP2 give the same order of sensitivity as the Fermilab Tevatron [2,3]. As an example, DELPHI has the 95% C.L. limits of $-0.46 < \Delta\kappa < 0.84$ and $-0.44 < \lambda < 0.24$. A combination of measurements of triple gauge boson couplings from the four LEP2 experiments improves the precision to $-0.09 < \Delta\kappa < 0.15$ ($\lambda=0$) and $-0.066 < \lambda < 0.035$ ($\Delta\kappa=0$) where $WWZ$ coupling is kept at the SM value for both cases [4]. Analyses of the $WW\gamma$ vertex has been given by several papers for the DESY $ep$ collider HERA [5–10]. The CERN Large Hadron Collider (LHC) is expected to place better limits on these couplings of $O(10^{-2})$ for $\Delta\kappa$ and $O(10^{-3})$ for $\lambda$ [11]. Linear electron-positron colliders (LC) will improve further upon the LHC precision by one order of magnitude [12].

Research and development on linear $e^+e^-$ colliders at SLAC, DESY, and KEK have been progressing and the physics potential of these future machines is under intensive study. After linear colliders are constructed $\gamma e$ and $\gamma\gamma$ modes with real photons should be discussed and may work as complementary to basic colliders [13,14]. The real gamma beam is obtained by the Compton backscattering of laser photons off the linear electron beam where most of the photons are produced at the high energy region. Since the luminosities for $\gamma e$ and $\gamma\gamma$ collisions turn out to be of the same order as the one for the $e^+e^-$ collision [15], the cross sections for photoproduction processes with real photons are considerably larger than the virtual photon case. Polarizability of the real gamma beam is an additional advantage for polarized beam experiments. In this paper we examine the capability of the $\gamma e$ mode of LC to probe the anomalous $WW\gamma$ coupling with polarized electron and gamma beams, assuming $W$ polarization will be measured [3].

## II. LAGRANGIAN AND CROSS SECTIONS

The $C$ and $P$ parity conserving effective Lagrangian for two charged $W$ bosons and one photon interaction can be written following the papers [17,18]:

$$\frac{iL}{g_{WW\gamma}} = g_1^\gamma (W^\dagger_{\mu\nu} W^\mu A^\nu - W^{\mu\nu} W^\dagger_\mu A_\nu) + \kappa W^\dagger_\mu W_\nu A^{\mu\nu} + \frac{\lambda}{M_W^2} W^\dagger_{\rho\mu} W^\mu_\nu A^{\mu\rho}, \tag{1}$$

where

$$g_{WW\gamma} = e, \quad W_{\mu\nu} = \partial_\mu W_\nu - \partial_\nu W_\mu,$$

and dimensionless parameters $g_1^\gamma$, $\kappa$, and $\lambda$ are related to the magnetic dipole and electric quadrupole moments. Within the standard model, at tree level, the couplings are given by $g_1^\gamma=1$, $\kappa=1$, and $\lambda=0$. For on-shell photons, $g_1^\gamma=1$ is fixed by electromagnetic gauge invariance to its standard model value at tree level. In momentum space this has the following form with momenta $W^+(p_1)$, $W^-(p_2)$, and $A(p_3)$:

$$\begin{aligned}\Gamma_{\mu\nu\rho}(p_1,p_2,p_3) = e\Bigg[ & g_{\mu\nu}\left( p_1 - p_2 - \frac{\lambda}{M_W^2}[(p_2.p_3)p_1 - (p_1.p_3)p_2] \right)_\rho \\ & + g_{\mu\rho}\left( \kappa p_3 - p_1 + \frac{\lambda}{M_W^2}[(p_2.p_3)p_1 - (p_1.p_2)p_3] \right)_\nu \\ & + g_{\nu\rho}\left( p_2 - \kappa p_3 - \frac{\lambda}{M_W^2}[(p_1.p_3)p_2 - (p_1.p_2)p_3] \right)_\mu \\ & + \frac{\lambda}{M_W^2}(p_{2\mu}p_{3\nu}p_{1\rho} - p_{3\mu}p_{1\nu}p_{2\rho}) \Bigg],\end{aligned} \tag{2}$$

*Corresponding author. FAX: +90 312 2232395. Email address: atag@science.ankara.edu.tr

 ©2001 The American Physical Society

where $p_1+p_2+p_3=0$. The process we investigate $\gamma e \to W\nu$ is described by two Feynman diagrams and only the $t$-channel $W$ exchange graph contributes $WW\gamma$ vertex. One should note that $\gamma e$ collision isolates $WW\gamma$ coupling but many processes in $e^+e^-$, $pp$, and $ep$ collisions include mixtures of $WW\gamma$ and $WWZ$ couplings.

The helicity-dependent differential cross section for the subprocess $\gamma e \to W\nu$ can be obtained in terms of helicity amplitudes $M_{\lambda_\gamma \lambda_W}$

$$\frac{d\hat{\sigma}(\lambda_\gamma,\lambda_W)}{d\cos\theta}=\frac{\beta}{32\pi\hat{s}}|M_{\lambda_\gamma\lambda_W}|^2, \tag{3}$$

$$M_{\lambda_\gamma\lambda_W}=\frac{e^2}{\sqrt{2}\sin\theta_W}\frac{\hat{s}}{\hat{s}+M_W^2}\sqrt{\beta}A_{\lambda_\gamma\lambda_W}, \quad \beta=1-\frac{M_W^2}{\hat{s}}, \tag{4}$$

where $\theta$ is the angle between incoming photon with helicity $\lambda_\gamma$ and the outgoing $W$ boson with helicity $\lambda_W$ in the c.m. frame, and $\theta_W$ is the Weinberg angle. $\hat{s}$ is defined as the center of mass energy of $\gamma e$ system. Reduced amplitudes $A_{\lambda_\gamma\lambda_W}$ are given as follows:

$$A_{--}=2\left[-\frac{2M_W^2}{\hat{s}}+1+\kappa+\lambda\frac{(1-\cos\theta)}{2}\right]\frac{\cos\frac{\theta}{2}}{(1-\beta_W\cos\theta)}, \tag{5}$$

$$A_{-+}=-\frac{\lambda\hat{s}}{M_W^2}(1-\cos\theta)\frac{\cos\frac{\theta}{2}}{(1-\beta_W\cos\theta)}, \tag{6}$$

$$A_{-0}=-\frac{\sqrt{2\hat{s}}}{M_W}[\kappa-1-\lambda\cos\theta]\frac{\sin\frac{\theta}{2}}{(1-\beta_W\cos\theta)}, \tag{7}$$

$$A_{+-}=\left[\frac{2M_W^2}{\hat{s}}+\kappa-1-\lambda\frac{(\hat{s}-M_W^2)}{M_W^2}\right]\times(1-\cos\theta)\frac{\cos\frac{\theta}{2}}{(1-\beta_W\cos\theta)}, \tag{8}$$

$$A_{++}=(1+\kappa)(1+\cos\theta)\frac{\cos\frac{\theta}{2}}{(1-\beta_W\cos\theta)}, \tag{9}$$

$$A_{+0}=-\frac{M_W}{\sqrt{2\hat{s}}}\left[4+\left(1+\frac{\hat{s}}{M_W^2}\right)(\kappa-1-\lambda\beta_W)\right]\times(1+\cos\theta)\frac{\sin\frac{\theta}{2}}{(1-\beta_W\cos\theta)}, \tag{10}$$

with

$$\beta_W=\frac{\hat{s}-M_W^2}{\hat{s}+M_W^2}. \tag{11}$$

Expressions (5)–(10) are in agreement with those of Ref. [8], except for an overall minus sign in front of Eq. (10) which does not influence the cross sections. It is clear from above expressions that for the anomalous couplings at high energies contribution of $\kappa$ to helicity amplitudes $A_{-0}$ and $A_{+0}$ grows with $\sqrt{\hat{s}}/M_W$ and terms in $A_{-+}$ and $A_{+-}$ containing $\lambda$ behave like $\hat{s}/M_W^2$. This is why the anomalous couplings have to show a form factor behavior at very high energies. Here we assume that the form factor structure does not depend on the momentum transfers at the energy region we consider.

The cross section can be connected to initial laser photon helicity $\lambda_0$ before Compton backscattering through the formula

$$\frac{d\hat{\sigma}(\lambda_0,\lambda_W)}{d\cos\theta}=\frac{1}{4}(1-P_e)\left[[1+\xi(E_\gamma,\lambda_0)]\frac{d\hat{\sigma}(+,\lambda_W)}{d\cos\theta}+[1-\xi(E_\gamma,\lambda_0)]\frac{d\hat{\sigma}(-,\lambda_W)}{d\cos\theta}\right], \tag{12}$$

where $P_e$ is the initial electron beam polarization and $\xi(E_\gamma,\lambda_0)$ is the helicity of the Compton backscattered photon [15,16]

$$\xi(E_\gamma,\lambda_0)=\frac{\lambda_0(1-2r)[1-y+1/(1-y)]+\lambda_e r\zeta[1+(1-y)(1-2r)^2]}{1-y+1/(1-y)-4r(1-r)-\lambda_e\lambda_0 r\zeta(2r-1)(2-y)}. \tag{13}$$

Here $r=y/[\zeta(1-y)]$, $y=E_\gamma/E_e$, and $\zeta=4E_eE_0/M_e^2$. $E_0$ is the energy of the initial laser photon and $E_e$ and $\lambda_e$ are the energy and the helicity of the initial electron beam before Compton backscattering. One should note that $P_e$ and $\lambda_e$ refer to different electron beams. The behavior of the helicity of backscattered photons can be observed from Fig. 1 as a function of their energy. From the figure we see that the backscattered photons reach maximum polarization at the highest energy region. For outgoing $W$ bosons we take into account the possibility that the transverse and longitudinal

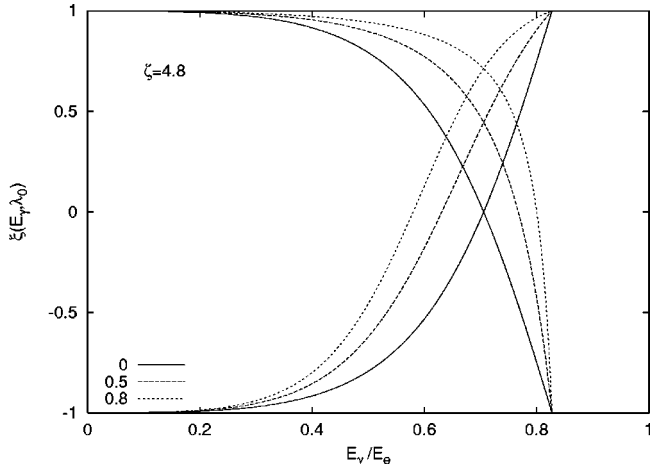


FIG. 1. Helicity of backscattered photons as a function of their energy. The set of curves starting from the bottom (upper) are plotted for $\lambda_0=-1$ ($\lambda_0=1$) and the legends are for helicities of the initial electron beam $\lambda_e$.

polarizations can be observed for each $\lambda_0$ state [3]. The cross sections which will be used in our calculations are as follows:

$$\frac{d\hat{\sigma}(\lambda_0,T)}{d\cos\theta}=\frac{d\hat{\sigma}(\lambda_0,+)}{d\cos\theta}+\frac{d\hat{\sigma}(\lambda_0,-)}{d\cos\theta}, \tag{14}$$

$$\frac{d\hat{\sigma}(\lambda_0,L)}{d\cos\theta}=\frac{d\hat{\sigma}(\lambda_0,0)}{d\cos\theta}, \tag{15}$$

where $T$ stands for transverse and $L$ for longitudinal. For the unpolarized beams the cross section takes the form

$$\frac{d\hat{\sigma}^{unpol}}{d\cos\theta}=\frac{d\hat{\sigma}(\lambda_0,T)}{d\cos\theta}+\frac{d\hat{\sigma}(\lambda_0,L)}{d\cos\theta} \tag{16}$$

with $\lambda_0=0$, $\lambda_e=0$, and $P_e=0$.

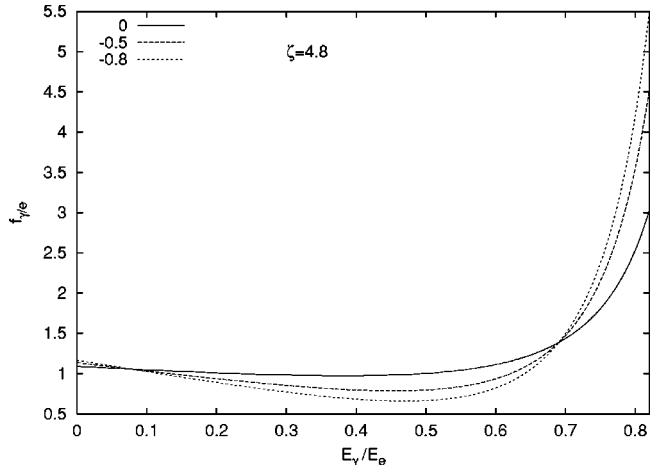


FIG. 2. Energy distribution of backscattered photons for $\lambda_0\lambda_e=0,\ -0.5,\ -0.8$.

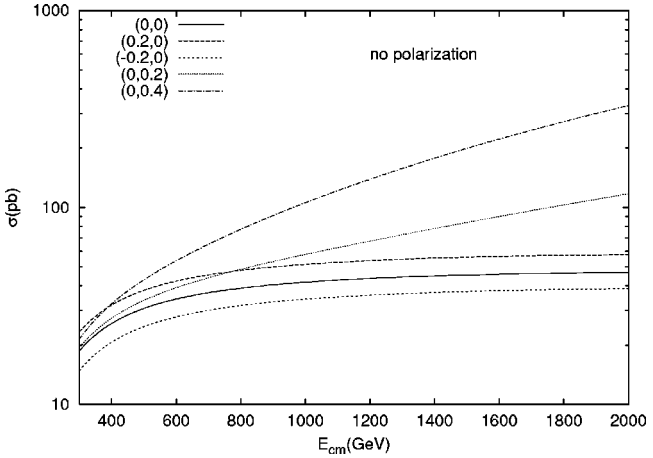


FIG. 3. Total cross sections versus the center of mass energy ($\sqrt{s}$) of the parental linear $e^+e^-$ colliders for the unpolarized case. The numbers in the legends stand for $(\kappa-1,\lambda)$.

For the integrated cross section, we need the spectrum of backscattered photons in connection with helicities of initial laser photon and electron which is given below [15,16]:

$$f_{\gamma/e}(y)=\frac{1}{g(\zeta)}\left[1-y+\frac{1}{1-y}-\frac{4y}{\zeta(1-y)}+\frac{4y^2}{\zeta^2(1-y)^2}+\lambda_0\lambda_e r\zeta(1-2r)(2-y)\right], \tag{17}$$

where

$$g(\zeta)=g_1(\zeta)+\lambda_0\lambda_e g_2(\zeta),$$

$$g_1(\zeta)=\left(1-\frac{4}{\zeta}-\frac{8}{\zeta^2}\right)\ln(\zeta+1)+\frac{1}{2}+\frac{8}{\zeta}-\frac{1}{2(\zeta+1)^2}, \tag{18}$$

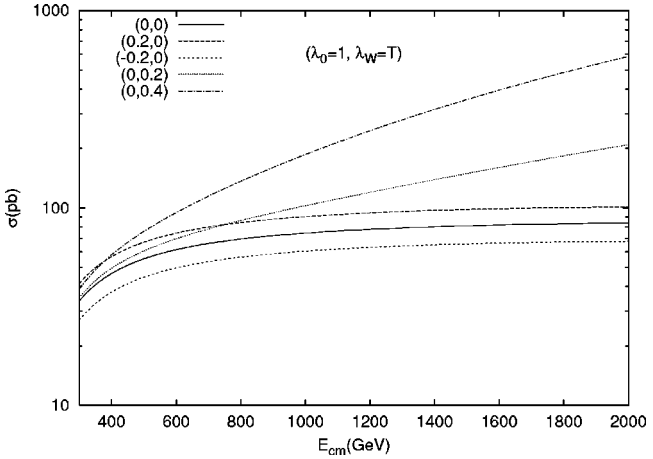


FIG. 4. The same as in Fig. 3 but for the polarization parameters $\lambda_0=1$, $\lambda_W=T$, and $P_e=-0.8$. $T$ and $L$ are for transverse and longitudinal polarization.

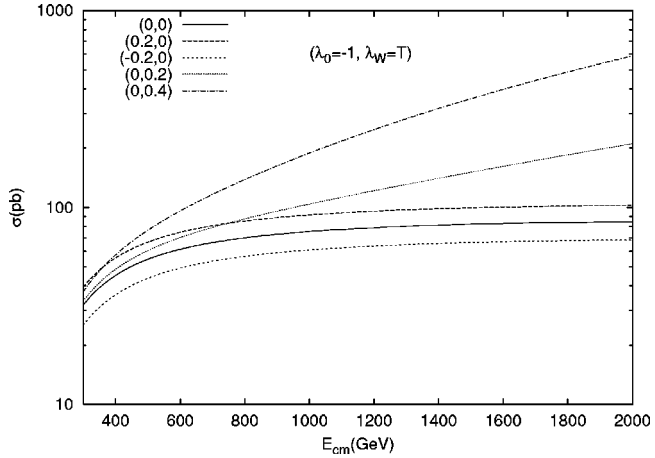


FIG. 5. The same as in Fig. 3 but for the polarization parameters $\lambda_0=-1$ and $\lambda_W=T$.

$$g_2(\zeta)=\left(1+\frac{2}{\zeta}\right)\ln(\zeta+1)-\frac{5}{2}+\frac{1}{\zeta+1}-\frac{1}{2(\zeta+1)^2}. \tag{19}$$

The definitions of $r$, $y$, and $\zeta$ are the same as in the helicity expression and the maximum value of $y$ reaches 0.83 when $\zeta=4.8$. To see the influence of polarization, energy distributions of backscattered photons $f_{\gamma/e}$ are plotted for $\lambda_0\lambda_e=0,\ -0.5,\ -0.8$ in Fig. 2. Using Eq. (17) and Eqs. (13)–(15) the integrated cross section over the backscattered photon spectrum is written below:

$$\frac{d\sigma(\lambda_0,\lambda_W)}{d\cos\theta}=\int_{y_{\min}}^{0.83} f_{\gamma/e}(y)\,\frac{d\hat{\sigma}(\lambda_0,\lambda_W)}{d\cos\theta}\,dy \tag{20}$$

with $y_{\min}=M_W^2/s$. Here $\hat{s}$ is related to $s$, the square of the center of mass energy of the $e^+e^-$ system, by $\hat{s}=ys$. In order to give an idea about the comparison of unpolarized and polarized cases, integrated total cross sections as functions of $\sqrt{s}$ are shown in Figs. 3–7 for various anomalous coupling values and different configurations of polarizations.

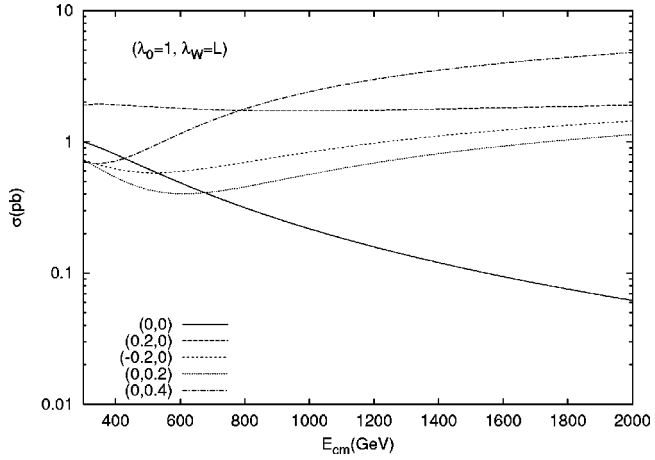


FIG. 6. The same as in Fig. 3 but for the polarization parameters $\lambda_0=1$ and $\lambda_W=L$.

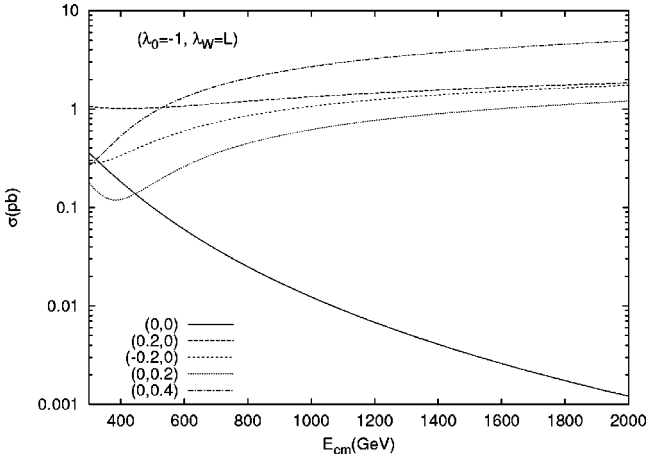


FIG. 7. The same as in Fig. 3 but for the polarization parameters $\lambda_0=-1$ and $\lambda_W=L$.

A common feature in each figure is that higher $\sqrt{s}$ will highly improve the sensitivity of the cross section to $\lambda$ when compared with $\kappa$. Cross sections are almost two times larger for the transverse $W$ case than those obtained in the unpolarized case. For the longitudinally polarized $W$ case, the magnitude of the total cross sections are smaller but the deviations in the total cross sections from the SM value seem larger than the case of transverse $W$. For completely polarized Compton backscattered photons the SM cross section would give zero with $\lambda_0=-1$ and $\lambda_W=L$, because the reduced amplitude $A_{-0}=0$ for the SM values of anomalous coupling parameters. Thus, the cross sections (or number of events) in Fig. 7, if observed, can possibly be taken as manifestation of anomalous couplings. It is seen that the longitudinal polarization state of the $W$ boson is more promising to make the deviations visible. A detailed statistical analysis will be given in Sec. III regarding the constraints on anomalous couplings.

It is also important to see how the anomalous couplings change the shape of the angular distribution of the $W$ boson

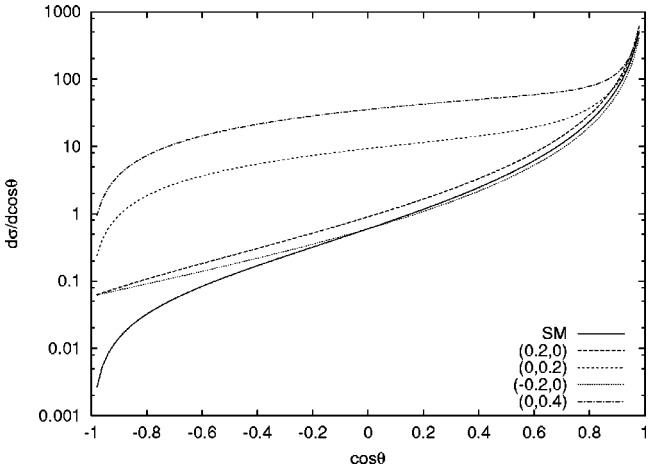


FIG. 8. $\kappa$ and $\lambda$ dependence of the angular distribution of the $W$ boson in the $\gamma e$ collision for the unpolarized case. The unit of the cross section is pb and the numbers in front of the legends stand for anomalous coupling parameters $(\kappa-1,\lambda)$. $\sqrt{s}=1$ TeV.

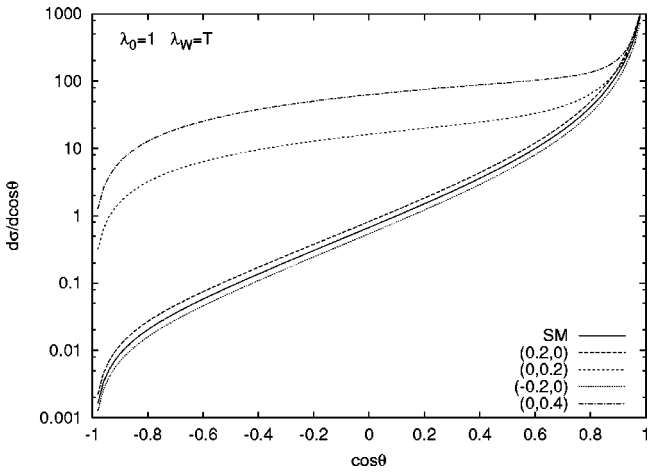


FIG. 9. The same as Fig. 8 but for the polarized case. The values of helicities of the initial laser photon and final $W$ boson $\lambda_0$, $\lambda_W$ are given on the graph.

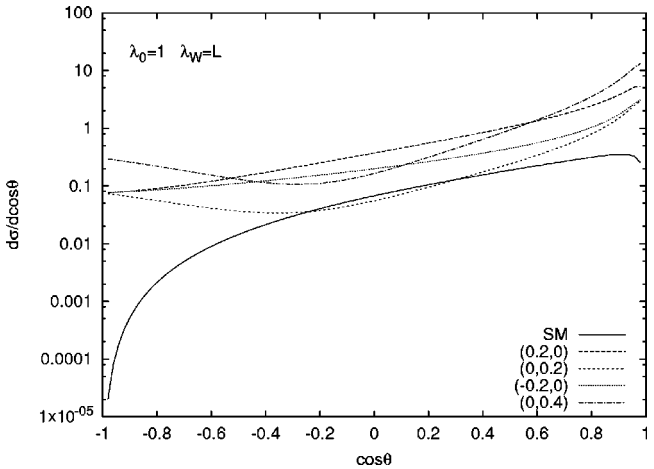


FIG. 10. The same as Fig. 8 but for the helicities shown on the graph.

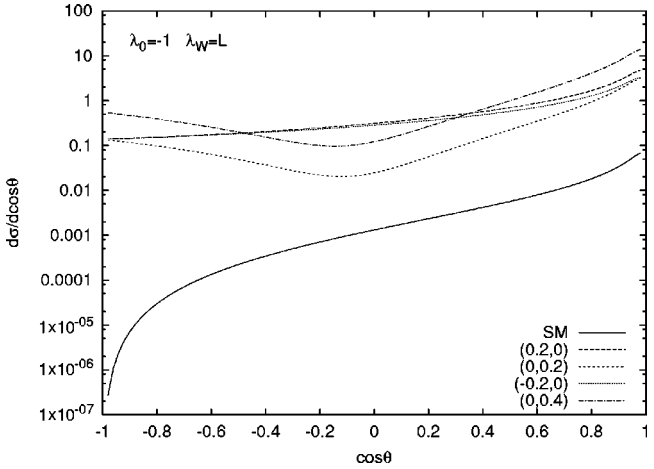


FIG. 11. The same as Fig. 8 but for the helicities shown on the graph.

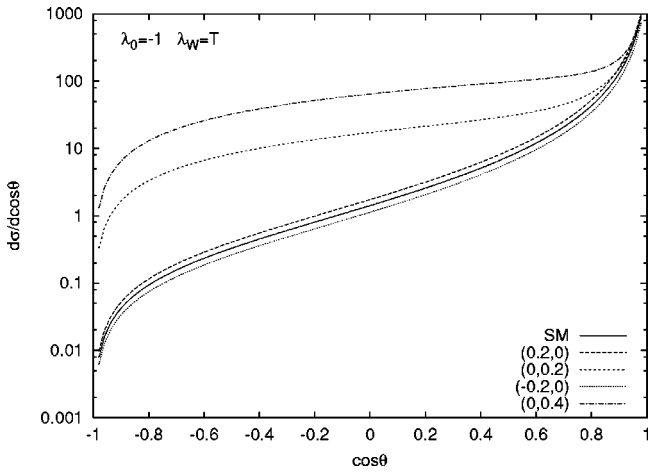


FIG. 12. The same as Fig. 8 but for the helicities shown on the graph.

for the polarized and unpolarized cases. We use integrated cross section, Eq. (20), to obtain angular distributions in Figs. 8–12. Similar features to total cross sections occur in angular distributions of the $W$ boson in terms of deviations from SM values of anomalous couplings. For simplicity, let us take into account the angular region transverse to beam direction $\theta \sim \pi/2$. In the unpolarized and transversely polarized $W$ boson distribution case, $\lambda$ dependence causes much more separation from the SM distribution compared to $\kappa$ dependence. In the longitudinally polarized $W$ boson case, separation due to the $\kappa$ dependence gets large together with the $\lambda$ dependence. Another difference arises in forward directions, $\cos\theta \sim 1$ between the transversely polarized case (or unpolarized case) where all curves approach each other, and the longitudinally polarized $W$ boson case where the SM curve deviates from all the other curves.

## III. SENSITIVITY TO ANOMALOUS COUPLINGS

Using the simple $\chi^2$ criterion from angular distribution we estimate sensitivity of the LC-based $\gamma e$ collider to anomalous couplings for the integrated luminosity values of 500 fb$^{-1}$ and $\sqrt{s}=0.5$, 1, 1.5 TeV:

$$\chi^2 = \sum_{i=bins} \left( \frac{X_i - Y_i}{\Delta_i^{exp}} \right)^2, \tag{21}$$

TABLE I. Sensitivity of the $\gamma e$ collider to anomalous couplings at 95% C.L. for $\sqrt{s}=0.5$ TeV and $L_{int}=500$ fb$^{-1}$. Only one of the couplings is assumed to deviate from the SM at a time.

| $\lambda_0$ | $P_e$ | $\lambda_W$ | $\Delta\kappa$ ($10^{-4}$) | $\lambda$ ($10^{-3}$) |
|---|---|---|---|---|
| 0 | 0 | $T+L$ | $-5$, 5 | $-8.0$, 8.0 |
| $+1$ | $-0.8$ | $T$ | $-4$, 4 | $-4.5$, 7.8 |
| $+1$ | $-0.8$ | $L$ | $-7$, 7 | $-0.8$, 0.8 |
| $-1$ | $-0.8$ | $T$ | $-4$, 4 | $-5.0$, 3.0 |

TABLE II. The same as Table I but for $\sqrt{s}=1$ TeV and $L_{int}=500$ fb$^{-1}$.

| $\lambda_0$ | $P_e$ | $\lambda_W$ | $\Delta\kappa$ $(10^{-4})$ | $\lambda$ $(10^{-3})$ |
|---|---|---|---|---|
| 0 | 0 | $T+L$ | $-4, 4$ | $-3.0, 3.0$ |
| $+1$ | $-0.8$ | $T$ | $-3, 3$ | $-1.9, 2.6$ |
| $+1$ | $-0.8$ | $L$ | $-6, 6$ | $-0.6, 0.6$ |
| $-1$ | $-0.8$ | $T$ | $-3, 3$ | $-3.7, 2.1$ |

TABLE III. The same as Table II but for $\sqrt{s}=1.5$ TeV and $L_{int}=500$ fb$^{-1}$.

| $\lambda_0$ | $P_e$ | $\lambda_W$ | $\Delta\kappa$ $(10^{-4})$ | $\lambda$ $(10^{-3})$ |
|---|---|---|---|---|
| 0 | 0 | $T+L$ | $-4, 4$ | $-1.7, 1.7$ |
| $+1$ | $-0.8$ | $T$ | $-3, 3$ | $-1.2, 1.3$ |
| $+1$ | $-0.8$ | $L$ | $-6, 6$ | $-0.6, 0.6$ |
| $-1$ | $-0.8$ | $T$ | $-3, 3$ | $-1.8, 1.4$ |

$$X_i=\int_{z_i}^{z_{i+1}}\frac{d\sigma^{SM}}{dz}dz,$$

$$Y_i=\int_{z_i}^{z_{i+1}}\frac{d\sigma^{NEW}}{dz}dz, \tag{22}$$

$$\Delta_i^{exp}=X_i\sqrt{\delta_{stat}^2+\delta_{sys}^2}, \quad z=\cos\theta. \tag{23}$$

We have divided the range of $\cos\theta$ into six equal pieces for the binning procedure and have considered at least 10 events in each bin. Using the above formula the limits on the $\Delta\kappa$ and $\lambda$ are given in Tables I–III for the deviation of the cross section from the standard model value at 95% confidence level without systematic error. Both limits on $\Delta\kappa$ and $\lambda$ can reach the order of $O(10^{-4})$. From these tables we see that the longitudinal $W$ production is more sensitive to the limits on $\lambda$ but the transverse $W$ production is more sensitive to $\Delta\kappa$. Comparison shows that the polarization improves the limits on $\Delta\kappa$ by a factors 1.3 and on $\lambda$ by factors 2.8–10.

The $\gamma e$ collider mode of LC probes $\Delta\kappa$ and $\lambda$ with better sensitivity than the present colliders, Fermilab Tevatron and LEP2 experiments, and than the future collider LHC which can probe $WW\gamma$ and $WWZ$ couplings separately with $W\gamma$ and $WZ$ production. It is anticipated that the future linear $e^+e^-$ colliders provide the sensitivity of $O(10^{-4})$, depending on the energy and luminosity with mixed couplings of $WW\gamma$ and $WWZ$ vertices for unpolarized beams [12]. The highly polarizable beams at LC allow one to discriminate couplings at the same order of sensitivity as above [19] that have correlated effects on observables with unpolarized beams. The satisfactory comparison between the sensitivities from $\gamma e\to W\nu$ and from the basic linear $e^+e^-$ collider should be discussed after the actual condition in the experiment, including uncertainty in the luminosity and detector, is taken into account. Previous limits from $\gamma e$ collisions with laser backscattering have been produced for the $WW\gamma$ couplings with $O(10^{-2})$ precision, using unpolarized beams [20] and polarization asymmetry zero [21]. The same order of constraints have also been obtained in the $\gamma\gamma$ collision for the unpolarized case in Ref. [20].

A reduction in luminosity is expected in the $\gamma e$ collision when compared to the basic $e^+e^-$ collision due to the scattering of laser photons. However, there are some possibilities for increasing luminosity using electron beams with low emittances [22].

As the complementary collider, the $\gamma e$ mode with the luminosity comparable to that in the $e^+e^-$ collision probes the $WW\gamma$ couplings independently of the $WWZ$ effects. With reasonable systematic error one expects to see the effects of the standard model radiative corrections. For more precise results, further analysis needs to be supplemented by observables such as the distributions of the $W$ decay products with a more detailed knowledge of the experimental performances.


[1] D0 Collaboration, B. Abbott *et al.*, Phys. Rev. D **60**, 072002 (1999).

[2] ALEPH Collaboration, R. Barate *et al.*, Phys. Lett. B **422**, 369 (1998); DELPHI Collaboration, P. Abreu *et al.*, *ibid.* **423**, 194 (1998); L3 Collaboration, M. Acciari *et al.*, *ibid.* **467**, 171 (1999); OPAL Collaboration, G. Abbiendi *et al.*, Eur. Phys. J. C **9**, 191 (1999).

[3] OPAL Collaboration, G. Abbiendi *et al.*, Eur. Phys. J. C **19**, 229 (2001).

[4] LEP Collaborations ALEPH, DELPHI, L3, OPAL, and The LEP TGC Working Group, G. Bella *et al.*, LEPEWWG/TGC/2000-01.

[5] M.N. Dubinin and H.S. Song, Phys. Rev. D **57**, 2927 (1998).

[6] U. Baur, J. Vermaseren, and D. Zeppenfeld, Nucl. Phys. **B375**, 3 (1992).

[7] C.S. Kim, Jungil Lee, and H.G. Song, Z. Phys. C **63**, 673 (1994).

[8] U. Baur and D. Zeppenfeld, Nucl. Phys. **B325**, 253 (1989).

[9] M. Janssen, Z. Phys. C **52**, 165 (1991); M. Böhm and A. Rosado, *ibid.* **39**, 275 (1988).

[10] V.A. Noyes, Proceedings of the Workshop on Future Physics at HERA 1995/96, edited by G. Ingelman, A. De Roeck, and R. Klanner (DESY, Hamburg, 1996), p. 190; S. Godfrey, Z. Phys. C **55**, 619 (1992); T. Helbig and H. Spiesberger, Nucl. Phys. **B373**, 73 (1992); U. Baur and M.A. Doncheski, Phys. Rev. D **46**, 1959 (1992).

[11] ATLAS Technical Design report, 1999, Vol. II.

[12] "The case for a 500 GeV $e+e-$ Linear Collider," hep-ex/0007022 by the American Linear Collider Working Group; TESLA Technical Design Report, Part III, "Physics at an $e+e-$ Linear Collider," edited by R.D. Heuer, D. Miller, F. Richard, and P.M. Zerwas, 2001, http://www.desy.de/ lcnotes/tdr

[13] C. Akerlof, Ann Arbor Report No. UM HE 81-59, 1981.

[14] T.L. Barklow, in Proceedings of the 1990 Summer Study on Research Directions for the Decade (Snowmass, Colorado, 1990), and SLAC Report No. SLAC-PUB-5364, 1990.
[15] I.F. Ginzburg *et al.*, Nucl. Instrum. Methods **205**, 47 (1983); **219**, 5 (1984).
[16] V.I. Telnov, Nucl. Instrum. Methods Phys. Res. A **294**, 72 (1990); D.I. Borden, D.A. Bauer, and D.O. Caldwel, SLAC Report No. SLAC-PUB-5715, 1992.
[17] K.J.F. Gaemers and G.J. Gournaris, Z. Phys. C **1**, 259 (1979).
[18] K. Hagiwara, R.D. Peccei, D. Zeppenfeld, and K. Hikasa, Nucl. Phys. **B282**, 253 (1987).
[19] V.V. Andreev, A.A. Pankov, and N. Paver, Phys. Rev. D **53**, 2390 (1995); A.A. Likhoded, T. Han, and G. Valencia, *ibid.* **53**, 4811 (1996).
[20] S.Y. Choi and F. Schrempp, Phys. Lett. B **272**, 149 (1991).
[21] S.J. Brodsky and T.G. Rizzo, Phys. Rev. D **52**, 4929 (1995).
[22] V. Telnov, Turk. J. Phys. **22**, 541 (1998).